



OPEN Study on the development pattern of continuous aquitard water-conducting fracture zones and rock layer detection borehole camera technology

Enyu Xu¹, Chao Xu¹, Xijian Li^{1,2}✉, Weiguang Zhou³, Xianzhong You³, Youping Peng³, Zewei Dong³, Chen Zou³ & Shoukun Chen^{1,2}

The northern part of Guizhou Province is rich in coal resources, but mining safety is threatened by water-bearing strata. This study zeroes in on Longfeng Coal Mine in Guizhou Province and delves into the issue of water damage in coal mines under complex geological conditions. By applying a range of methods—empirical formulas for water-conducting fracture zones from massive data fitting, overburden theory, numerical simulation, DC electrical method exploration, and borehole camera detection—the study reveals that as the working face advances, the overburden fracture zone expands sideways and compacted in the middle. The fractal dimension of the water-conducting fracture zone fluctuates remarkably, showing a clear link to water inrush. Based on fracture development patterns, an integrated surface and underground exploration drilling scheme was designed and carried out. The scheme successfully determined that the water-conducting fracture zone's development height was between 44 and 59 m, with a fracture-to-mining ratio of 15.39–20.63. The detachment water accumulation space lies in the hard-soft interlayer formed by the Longtan group limestone and the underlying silty mudstone. In engineering practice, the rock-layer detection borehole camera was upgraded. Its image-presentation effect was optimized, and the detection depth of the borehole was increased. Additionally, a multi-angle detection borehole camera with waterproof, mud-proof, and cold-resistant capabilities was designed, and technical improvement measures were proposed to adapt to more complex underground conditions and ensure more accurate rock-layer information acquisition. These innovations provide significant guidance and reference for preventing water inrushes in mines and protecting groundwater resources under similar geological conditions.

Keywords Groundwater resources, Water hazard prevention and control, Water-conducting fracture zones, Coal seam mining simulation, Rock layer detection

China's Guizhou Province, known as the "Coal Sea of South China", is the province with the most abundant coal resources among southern Chinese provinces. It has a proven coal reserve of 54.228 billion tons, accounting for 61% of southwest China's total and exceeding the combined reserves of 12 southern provinces (autonomous regions and municipalities). Its coal production exceeds 100 million tons annually. However, Guizhou's coal resources are faced with the threat of water disasters due to the province's intricate geological framework¹⁻³. Moreover, the distinctive karst landscape typical of Guizhou exacerbates the risk of such hazards, given its susceptibility to the creation of caverns and subterranean watercourses. The unexpected outflow of water from these geological features during mining activities poses significant threats to safety^{4,5}. As the initiative for ecological civilization progresses, addressing the issue of water hazard mitigation while ensuring the sustainable exploitation of coal and the conservation of groundwater has become increasingly critical. The resolution of this issue is pivotal not only for the enduring growth of the coal sector but also for safeguarding the ecological security and the welfare of the Guizhou region⁶⁻⁸.

¹College of Mining, Guizhou University, Guiyang 550025, Guizhou, China. ²Key Laboratory of Karst Georesources and Environment (Guizhou University), Ministry of Education, Guiyang 550025, PR China. ³Guizhou Jinsha Longfeng Coal Industry Co., Ltd, Bijie 551700, Guizhou, China. ✉email: xjli1@gzu.edu.cn

Analyzing the development of water-conducting fractures within aquifers is vital for the prevention and mitigation of water-related mining hazards, as well as for the conservation of groundwater resources. A variety of scholarly activities have been conducted, including theoretical exploration, experimental research, and field measurements⁹. Investigative methods span overburden mechanics¹⁰¹¹; empirical formulas¹⁰¹²; simulation experiments¹³¹⁴; numerical modeling^{1214–16}; and on-site testing¹²¹⁵¹⁷¹⁸;;. In China, the height of water-conducting fractures in the roof above coal seams is generally determined by a formula from the ‘Regulations for the Preservation of Coal Pillars for Buildings, Water Bodies, Railways, and Main Transportation Coal Columns, as well as Coal Mining’¹⁹. This empirical formula, based on data from various mining thicknesses, may not account for all influencing factors, leading to potential inaccuracies²⁰. To achieve a more accurate understanding of fracture development, researchers have integrated various methods, resulting in a broad array of insights. A mathematical model has assessed how different geological conditions affect the spread of fractures during multi-cluster fracturing in horizontal wells²¹. With increased mining progression, the deformation and breakdown of the overlying rock layers lead to a rising density and height of fractures²². The thickness of the mined coal seam and the characteristics of the rock layers above significantly influence the Water-conducting Fractured Zone (WCFZ), with the width of the mining face also playing a role²³. For steep coal seams, the WCFZ range is largely affected by factors including the length of the filling area beneath the goaf, changes in the roof rock, the coal seam’s inclination, the mining face length, and the load from the overburden²⁴. Transient electromagnetic technology has been found feasible for aquifer location detection, and the combined use of seismic and transient electromagnetic (CSAMT) inversion techniques can more accurately identify water-rich zones and their distribution in sandstone layers beneath low-resistance sandstone²⁵²⁶. By applying fractal theory and calculating the elongation rate of the mudstone layers within the rock strata, the development patterns of fractures can be quantitatively analyzed^{27–29}. Machine learning has become a key forecasting method, with scholars using models such as genetic algorithms, support vector machines, fusion models, and intelligent optimization algorithms to predict the height of water-conducting fractured zones, demonstrating high practicality^{30–32}.

Many methods and rich achievements have been accumulated in the research field of aquifer and water-conducting fracture zone. However, due to the complexity of mine conditions, the numerical simulation of water-conducting fracture formula and three-zone development can only stay at the theoretical level, and the transient electromagnetic detection technology can only partially reveal the water-bearing characteristics of rock strata. Under the condition of low temperature and high water, the detection effect of the rock formation detector is not satisfactory. Generally speaking, these research methods have not achieved the expected effect in practical application.

In light of this, taking the LF coal mine as an example, comprehensively applied various methods, including empirical formulas for water-conducting fracture zones derived from massive data fitting, overburden theory, and numerical simulation, among other methods, to serve on-site construction and design exploration technical schemes under complex conditions such as continuous aquifers. Further, combining direct current electrical method exploration with integrated surface and underground detection technology, this paper conducts a comprehensive analysis of the development patterns of continuous aquifer water-conducting fracture zones. On this basis, considering the mine’s rock conditions and geological environment, a waterproof and mud-proof detection borehole camera was upgraded. Additionally, a multi - angle detection borehole camera with waterproof, mud - proof, and cold - resistant capabilities was designed. The goal of applying this equipment was to offer practical guidance for preventing and controlling water inrush in mines with similar geological conditions. Through these measures, this paper not only enhances the scientific and practical aspects of mine water hazard prevention and control but also offers new solutions for mine construction and safety under similar complex conditions.

Engineering background

LF coal mine is located in Jinsha County and Qianxi City, Guizhou Province. The primary mining area currently is the 1903 working face of the coal seam. This working face is situated in the southwestern part of the mining area’s first mining district, with its strike length ranging between 1261.5 m and 1310.9 m and a dip width of 200.5 m. The working face has an inclination angle between 5 and 13 degrees, averaging 8 degrees. The No. 9 coal seam has a thickness that varies from 2.2 to 3.3 m, with an average burial depth of 417 m. The structure of the No. 9 coal seam is relatively simple, typically free of intercalated rocks, although it may contain 0 to 2 layers of intercalated rocks in the merged areas, which are generally carbonaceous mudstones. The No. 9 coal seam is one of the main minable coal seams in the minefield. The roof and floor of this coal seam are mainly composed of mudstone, siltstone, or sandy mudstone, which are geologically stable and minable throughout the entire area. The geological drillhole’s columnar diagram is displayed in Fig. 1, further illustrating the geological conditions of the coal seam.

The 1903 working face is arranged in the direction of the coal seam’s inclination and is mined using the inclined longwall mining method, which is a retreat mining face with the roof managed by the complete caving method. During the mining period, the working face is primarily threatened by water hazards from the overlying aquifers, with the maximum water inrush volume reaching 216 cubic m per hour, while the normal inrush volume is 86.4 cubic m per hour. The direct water-charging source of the working face is the aquifers from the LT group’s top limestone and the CX Formation’s limestone. It is worth noting that the CX Formation’s limestone aquifer and the LT group’s top limestone aquifer are actually the same water-bearing body and are in direct contact, and both are developed in karst geological environments..

Karst geological conditions play a significant role in influencing the development of fracture zones in this area. The dissolution of limestone by groundwater creates a large number of karst pores, cavities, and channels, which provide favorable space for the expansion and connection of fractures. Under the action of mining-induced stress, the original karst fractures are more likely to expand and form interconnected water-conducting fracture

Depth (m)	Histogram	Lithologic characters	Lithological description
18.11		Sandy mudstone	The primary strata consist of thin-bedded silty mudstone, argillaceous siltstone.
42.56		CX group limestone	Water-bearing layer: The primary geological feature is gray to dark gray, thickly bedded limestone, characterized by well-developed fractures and minor karstic cavities, which provide ample space for water infiltration.
57.15		LT group limestone	Water-bearing layer: The predominant rock type is gray to dark gray, medium-thick bedded bioclastic limestone, with well-developed fractures and minor karstic caves. Historical drilling operations in the area have encountered water inrushes.
59.76		Silty mudstone	Impermeable layer: It is widely distributed and is characterized by lithologies dominated by mudstone, limestone, and siltstone. It exhibits low water richness, making it suitable as a relatively impermeable layer.
61.35		Limestone	
76.38		Mudstone	
79.66		Limestone	
86.54		Sandy mudstone	
95.22		Siltstone	
95.72		Coal	
101.72		Muddy siltstone	The coal is predominantly bright coal, with secondary occurrences of mirror coal and dull coal, displaying a metallic sheen. It commonly features scattered crystalline pyrite and pyrite concretions. The coal exhibits a blocky texture with a wide to medium handed structure.
104.52		Coal	
132.26		Siltstone	The upper part is primarily composed of siltstone and sandy mudstone.

Fig. 1. Integrated Geological Drillhole Column Graph.

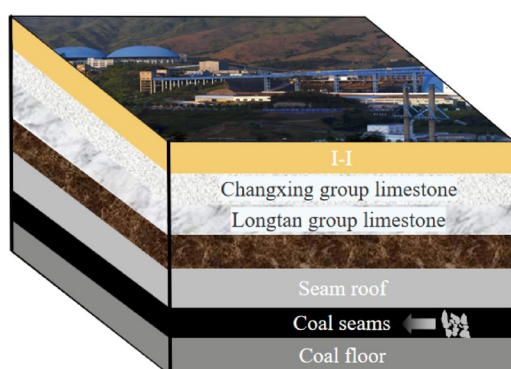


Fig. 2. Model of the Water-Conducting Channel.

networks, accelerating the development of water-conducting fault zones. Moreover, the uneven distribution of karstification leads to differences in the mechanical properties of the rock mass, resulting in uneven development of fracture zones—areas with strong karstification are more prone to form dense fracture clusters, which become key sections for groundwater migration. This interaction between karst and fractures makes the water-conducting channels more complex, increasing the difficulty of predicting water inrush hazards.

The water-conducting channels mainly consist of mining-induced fractures and fault fractures, which connect the water-rich areas of the aforementioned aquifers, allowing water from the aquifers to enter the working face through these channels. The water in these aquifers is replenished by the water source of the aquifers and atmospheric precipitation. Figure 2 illustrates the water-conducting channel conditions of the working face. To ensure safe coal mining under the water body, it is necessary to conduct in-depth research on the height of the WCFZ of the working face. This research is crucial for designing measures to prevent and control roof water hazards, as it provides the necessary parameters.

Research method

Empirical formula for WCFZ

The empirical formula for the WCFZ enables the prediction of the WCFZ's height, a phenomenon that arises from mining operations during coal extraction. Various factors contribute to the emergence of this fracture zone, such as the thickness of the mined coal, the area of the goaf (gob area), the types of overlying rock strata, the strategies for managing the roof, the state of the coal seam's storage, and the conditions of the mining environment. These elements are intricate, challenging to measure directly, and often display nonlinear behaviors. Consequently, the formulation of the empirical formula typically relies on a substantial dataset derived from actual observations, followed by statistical regression analysis to establish a reliable model³³³⁴.

Overburden theory

In the realms of mining and underground engineering, the Key Stratum Theory holds a significant position within the discipline of coal and rock mechanics. The theory is primarily concerned with the impact of rock strata configurations on surface subsidence and the diverse patterns of damage and movement that the overburden experiences during subterranean excavation. Central to the Key Stratum Theory is the identification and analysis

of pivotal rock strata that significantly influence the mining process. These critical layers are essential for managing surface subsidence and ensuring the structural integrity of underground construction projects^{35,36}.

To determine whether a particular rock layer is a key stratum, it can be identified using the following formula³⁷:

$$(q_n)_1 = \frac{E_1 h_1^3 (\gamma_1 h_1 + \gamma_2 h_2 + \dots + \gamma_n h_n)}{E_1 h_1^3 + E_2 h_2^3 + \dots + E_n h_n^3} \tag{1}$$

$$l_i = h_i \sqrt{\frac{2\sigma_i}{q_i}} \tag{2}$$

$$l_k < l_{k+1} \tag{3}$$

Where q_p , h_p , γ_p , E_p , σ_p , l_i and n refer to the load, thickness, volume weight, elastic modulus, tensile strength, breaking span and layers of the i^{th} layer, respectively.

During the mining process in coal mines, as the influence of mining activities gradually spreads, the WCFZ in the overburden rock layers continues to expand until it reaches the aquifer. This process leads to the infiltration of groundwater through the fracture zone, thereby causing seepage phenomena. To gain a deeper understanding of this phenomenon, the conceptual model of the overburden fracture field and the flow field helps to simplify the complexity of the geological structure in the study area, making the research work more efficient and targeted³⁸.

$$H_W = H_G - h_W \left(\frac{1}{\tan \theta_1} - \frac{1}{\tan \theta_2} \right) \tag{4}$$

In the formula: H_G represents the advance distance of the working face; h_W denotes the height of the aquifer; θ_1 is the fracture angle of the overburden above the entry cut; θ_2 is the fracture angle of the overburden above the working face.

Incorporating material mechanics and elasticity theory, the fracture angle of the overburden is calculated based on the initial fracture and periodic fracture step distance of the bedrock³⁹:

$$\begin{cases} \theta_1 = 45^\circ - \frac{\varphi}{2} + \frac{1}{2} \arctan \sqrt{\frac{18\sigma_t}{q}} \\ \theta_2 = 45^\circ - \frac{\varphi}{2} - \frac{1}{2} \arctan \left(-\sqrt{\frac{12\sigma_t}{q}} \right) \end{cases} \tag{5}$$

In the formulas: φ represents the angle of internal friction of the rock; σ_t denotes the tensile strength of the rock; q is the load above the rock layer.

Incorporating the actual mining conditions and advancement length of the 1903 working face at the LF coal mine, key stratum formulas 1–3, the aquifer disturbance distance formula 4, and the fracture angle formula 5 were used to derive the structural param of the ‘step-terrace’ model for the overburden fracture-seepage field. Furthermore, based on the measured flow rates and velocities, the seepage areas were clearly delineated. As shown in Fig. 3, corresponding control and prevention strategies were formulated according to the degree of damage to the rock layer support structure and the division of the seepage areas. These measures aim to reduce the collection of surface water and prevent water channels from seeping water into the aquifer, thereby avoiding

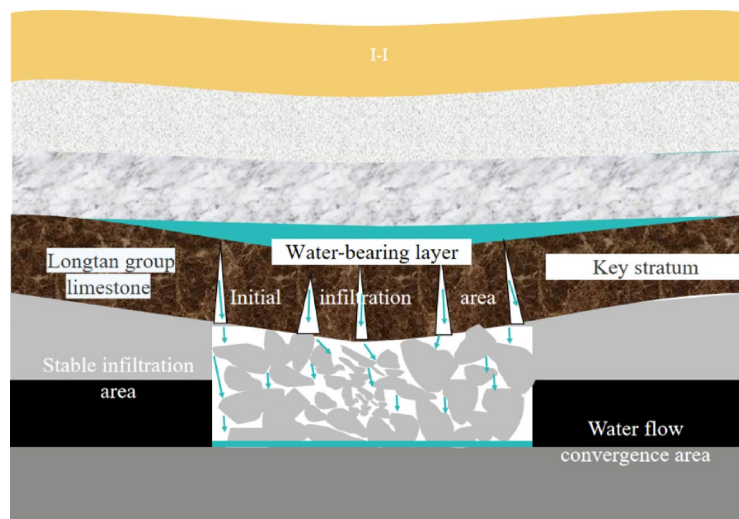


Fig. 3. Overburden Water-conducting Fracture Model.

breakthrough water inrushes caused by substantial recharge to the aquifer and preventing the formation of new strong permeability water inrush passages.

Numerical simulation

The UDEC (Universal Distinct Element Code) software (VERSION 6.0, <https://www.itasca.cc/xzsq>), a prominent tool in the fields of geotechnical, geological, and mining engineering, offers robust numerical simulation capabilities. Utilizing the Discrete Element Method (DEM), UDEC effectively models the intricacies of the coal mining process, encompassing activities such as tunneling, coal face progression, and the development of goaf zones. Beyond the excavation process, it also captures the subsequent stress redistribution and the resulting surface deformations, which are pivotal for evaluating the scope and effects of ground subsidence above mining areas. This capability is instrumental in the comprehensive assessment of mining-induced subsidence impacts⁴⁰.

Direct current (DC) electrical prospecting

Originating in the Soviet Union during the 1950s, the direct current electrical method of exploration is a technique that scrutinizes the electric field in the vicinity of a tunnel to identify geological formations. This approach capitalizes on the variance in electrical conductivity among different rock types. By establishing an electric field under the assumption of a full-space environment, a consistent electric field is induced within the rock layers encircling the tunnel through the use of power supply electrodes. The method is adept at uncovering water-bearing zones within the rock strata. Furthermore, by fine-tuning the spacing between the power supply electrodes, it is possible to investigate the geological structures at varying depths, thus furnishing vital data for geological surveys^{41,42}.

Rock layer detection instrument

The YTJ20, a specialized instrument for detecting rock layers, is designed for capturing images in underground boreholes. Employing an explosion-proof video recording setup, this method involves inserting a camera deep into the borehole to document its internal structure. The footage obtained is then transferred to surface media devices for detailed observation and analysis. By examining the recorded video, one can discern various geological features including lithology, fractures, voids, and weak interlayers present within the borehole. This visual data is instrumental for assessing the integrity of the overlying rock strata and serves as a foundation for estimating the extent of fracture development⁴³.

The JL-IDOI(A) intelligent borehole imaging instrument is a state-of-the-art device in geological exploration, designed for comprehensive underground borehole observation. It leverages digital signal processing (DSP) technology to acquire and process images with high precision. The instrument stands out for its ability to deliver high-definition and realistic imagery. Equipped with automatic calibration features for orientation and depth, it ensures accurate and detailed imaging of various borehole types, including vertical, horizontal, inclined, and those at multiple angles^{44,45}.

Results and discussion

Empirical formula calculation for WCFZ

Considering the geological context of the retreat mining at the 1903 working face, the maximum mining thickness of the coal seam is estimated to be between 2.2 and 3.3 meters. This is complemented by a caving rock expansion coefficient of 1.2 and an average inclination angle of the coal seam at 8 degrees. Geological assessments from the 1903 working face reveal that the immediate roof is composed of argillaceous siltstone, the main roof of sandstone, and the false roof of mudstone. The immediate floor beneath the coal seam is identified as carbonaceous mudstone, and the main floor is silty mudstone. The roof of the coal seam is categorized as moderately hard and is managed through the complete caving method. In accordance with the 'Guidelines for the Retention of Coal Pillars for Buildings, Water Bodies, Railways, and Main Shafts and the Mining of Pressurized Coal' from the 2017 edition, the development height of the WCFZ has been forecasted. This prediction serves as a guiding principle for the planning and layout of exploration boreholes, ensuring a more strategic and informed approach to mining operations¹⁹.

Calculation formula 1:

$$H_{li} = \frac{100 \sum M}{1.6 \sum M + 3.6} \pm 5.6 \quad (6)$$

H_{li} : Height of the WCFZ induced by coal seam mining, m; M : Mining thickness of coal seam; Based on the geological coal seam thickness of the 1903 working face, the minimum mining height is taken as 2.2 m, the maximum mining height as 3.3 m, and the average mining height as 2.86 m.

Calculation formula 2:

$$H_{li} = 20\sqrt{M} + 10 \quad (7)$$

According to the calculations, Formula (6) predicts the height of the WCFZ to range from 30.9 to 46.35 m, with a possible error of ± 5.6 m. Formula (7) provides an estimate of the fracture zone height between 39.66 and 46.33 m. The combined results from both formulas indicate that the development range of the water-conducting fracture zone is between 35.3 and 51.95 m below the floor of the No. 9 coal seam. Consequently, the design depth for the underground exploration boreholes should fall within this range. For a more comprehensive study of the development range of the WCFZ, numerical simulation research should be undertaken to ascertain the precise positioning of the exploration boreholes.

Lithology	Density (kg/m ³)	Bulk modulus (GPa)	Tension (MPa)	Cohesion (MPa)	Internal friction Angle (°)
Mudstone	2200	6.3	5.50	1.04	35
Siltstone	2500	12.5	3.00	4.16	38
Limestone	2580	12.5	4.90	3.96	41.8
Coal	1350	2.08	1.00	1.20	20
Silty mudstone	2250	6.25	2.60	1.46	34
Sandy mudstone	2290	7.25	1.46	1.46	38
Muddy siltstone	2450	10.25	2.26	1.86	34

Table 1. Physical and mechanical parameters of coal strata.

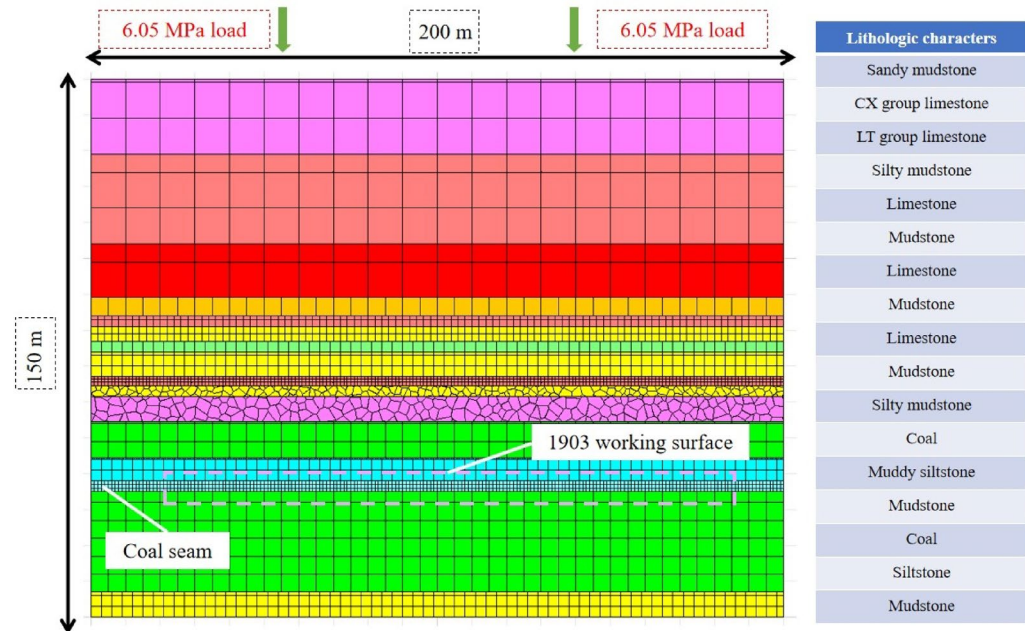


Fig. 4. Simplified Numerical Simulation Graph.

Analysis of numerical simulation research results

In an effort to delve deeper into the development pattern of the WCFZ at the LF coal mine's 1903 working face, a numerical simulation model was constructed using the UDEC discrete element software, grounded on the drilling column diagram of the working face. To streamline the simulation process, the advancement of the working face was simulated in four equal increments of 45 m, totaling 180 m. To mitigate the influence of boundary effects, a 10 m wide coal pillar was preserved along the sides of the model. Drawing from the theoretical calculation values pertaining to the mine's WCFZ, the model's height was designed to encompass the middle and upper sections of the LT group, culminating in a model height of 150 m. Given that the No. 9 coal seam's average burial depth is 417 m, an equivalent load of approximately 6.05 MPa was imposed on the model's upper surface, calculated using the formula for vertical stress. The model's final dimensions were established as 200 m in length and 150 m in height, with the top boundary set as free and all other boundaries fixed. The rock mass's constitutive relationship was defined by the Mohr-Coulomb failure criterion, while the behavior of joints and fractures was modeled using the Coulomb sliding model. The numerical calculation model and parameters are shown in Table 1; Fig. 4.

In the simulation, the longwall retreat advanced 15 m for each step. At the points of optimal fracture development (45, 90, 135, and 180 m from the working face), the extensibility of the overlying strata and the fracture characteristics are shown in Fig. 5.

The development of fractures in the overburden exhibits a distinct pattern of lateral development and central re-compaction within the coal seam goaf area. During the advancement of the working face, the overburden detachment has experienced the initiation and compaction closure of the detachment space. The specific process is as follows:

When the coal seam is advanced by 45 m (as shown in Fig. 5a), the rock layer activity is minimally affected by mining operations. The sandstone layer of the roof collapses, and the WCFZ has not yet penetrated the water-bearing LT group limestone, resulting in no significant water inrush at the working face at this time.

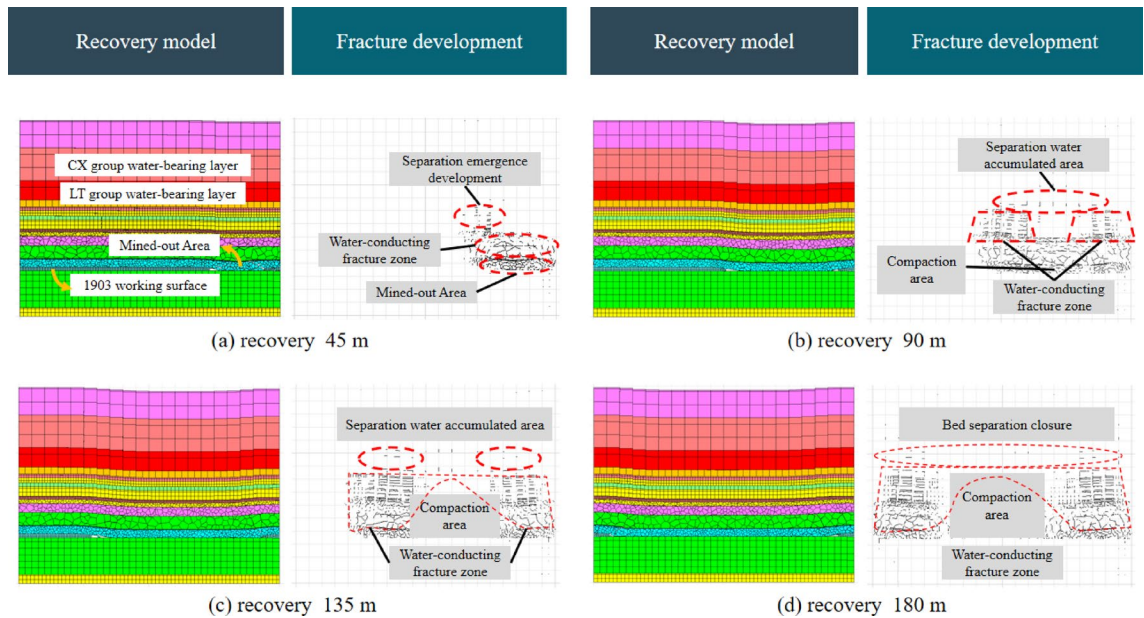


Fig. 5. Characteristics of Overburden Detachment and Fracture Development.

When the coal seam is advanced to 90 m (as shown in Fig. 5b), the development of the water-conducting fracture zone in the overburden rapidly expands in all directions, with significant rock layer activity influenced by mining operations. The WCFZ reaches the LT group limestone and the water accumulation area within the LT group's detachment space. Static water stored in the fractures and some of the water from the detachment zones flow into the working face through the WCFZ, causing a sudden increase in the instantaneous water inrush volume at the working face.

When the working face advances to 135 m (as shown in Fig. 5c), under the influence of mining activities, the original detachment space at the bottom of the LT group closes, while a new water accumulation area in the detachment zone forms in the middle of the LT group strata. The WCFZ continues to develop laterally, and the static water stored in the fractures is continuously released, flowing into the working face. A compacted fracture zone in the overburden appears in the middle of the goaf area.

When the working face advances to 180 m (as shown in Fig. 5d), the WCFZ in the overburden no longer develops upward but develops laterally, with the center being compacted. As the working face further advances, new detachment water accumulation areas are formed in the LT group limestone, and the rear detachment spaces are continuously compacted. Detached water intermittently flows into the working face through the water-conducting fracture zone.

The complexity of the fracture field distribution in the overburden, a consequence of coal seam mining, is well-documented. Studies have demonstrated that employing the fractal dimension method allows for a quantitative assessment of the development of fractures within the overburden that are induced by mining. The formula for calculating the fractal dimension is cited as follows⁴⁶:

$$D = \lim_{s \rightarrow 0} \frac{\lg N(r)}{-\lg r} \quad (8)$$

D represents the fractal dimension, while $N(r)$ denotes the number of grid cells containing fractures within a square grid of side length r . Here, r is the scale of the grid cell side length.

By processing the images of the fracture network in the overburden at different mining advance distances, the distribution pattern of the fractal dimension of the WCFZ in the overburden, influenced by mining disturbances, has been obtained, as shown in Fig. 6.

Due to the influence of rock layer movement in the middle of the goaf, the WCFZ is re-compacted, lacking a significant distribution of the WCFZ. This results in a lower fractal dimension of the fracture network in this area compared to the main water-conducting fracture channel. As the advance distance of the working face increases, new water-conducting fracture channels appear in the overburden ahead of the working face, while the existing water-conducting fracture channels begin to close due to compaction. This change leads to a decrease in the fractal dimension of the original WCFZ. With the continuous forward movement of the main water-conducting fracture channel ahead of the working face, the distribution of the fractal dimension in the overburden shows regular fluctuations and evolutionary characteristics.

To analyze and study the displacement changes of the water-bearing LT group limestone, displacement monitoring lines were laid out along the bottom of the rock layer. Each monitoring line was positioned based on the retreat distance of the coal seam, with 19 monitoring points established in the No. 9 coal seam to observe the

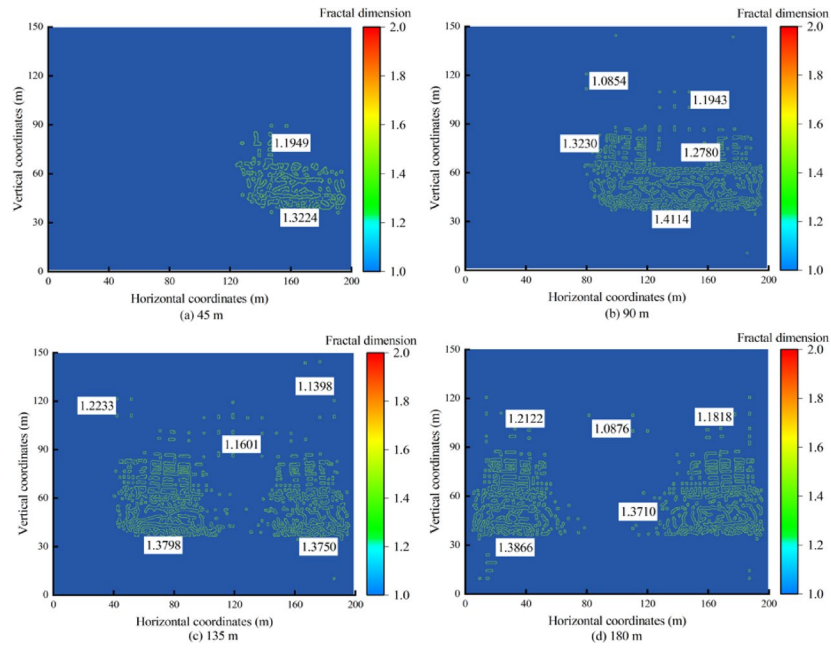


Fig. 6. Distribution of Fractal Dimension in the Overburden Fracture Network.

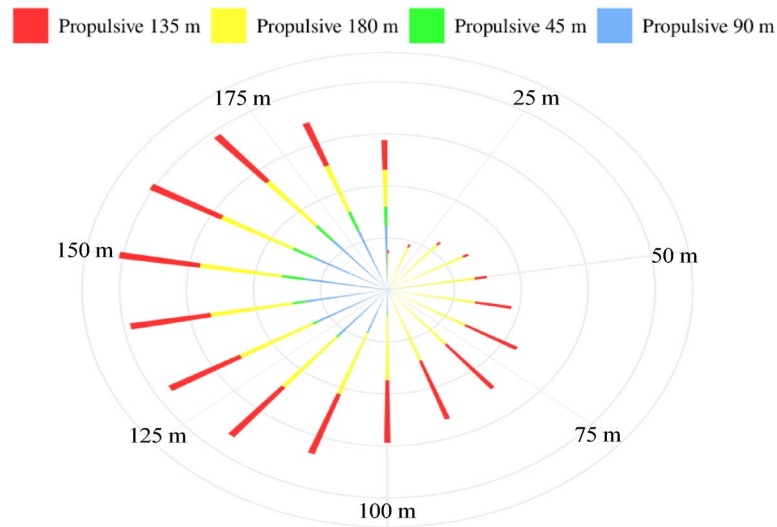


Fig. 7. Displacement Variation of LT Group Limestone.

displacement changes after the retreat mining of the working face. The displacement change graph was created, as shown in Fig. 7.

Based on the color and length in the rose diagram, it can be observed that the maximum subsidence displacement of the LT group limestone occurs at a 135-meter advance distance, followed by 180 m and 90 m, with the smallest displacement at 45 m. This indicates that at an advance distance of 45 m, fractures in the LT group limestone begin to develop; at 135 m, a detachment space is formed; after 180 m, the fractures are compacted over a small range, reducing the detachment space. The study concludes that after the coal seam experiences the initial stress, it is necessary to conduct actual measurement observations of fracture development in the aquifer to prevent and control water hazards; in the middle and late stages of coal seam retreat mining, the detachment space begins to develop, and attention should be paid to the development of the water accumulation space in the aquifer, for which rock layer water conduction prevention and control measures should be taken.

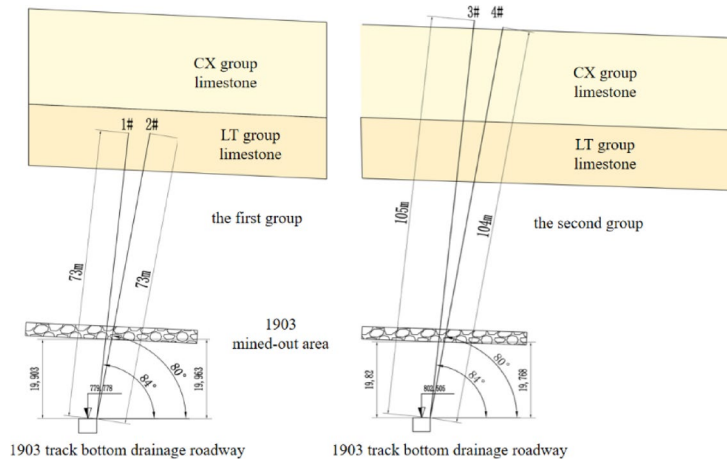


Fig. 8. Section View of Observation Drill Hole Layout.

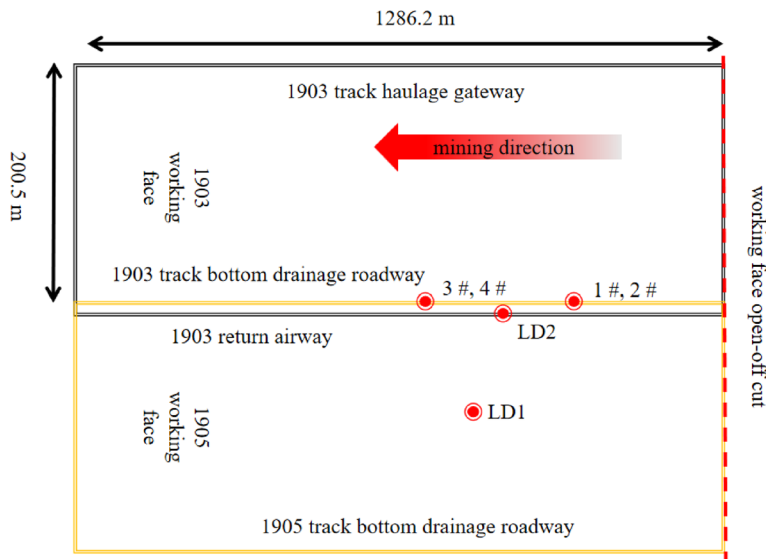


Fig. 9. Plan View of Ground Drill Hole Locations.

Analysis of On-Site measurement results

Underground borehole television survey construction locations

To accurately measure the height of the WCFZ in the No. 9 coal seam retreat mining and to effectively guide the mine’s water prevention and control efforts, observation holes for the “WCFZ” were constructed at the 1903 track bottom based on site conditions, results from empirical formula calculations, and numerical simulation outcomes. A set of four drill holes was constructed at retreat distances of 300 m and 500 m, with each set comprising two holes. All drill holes were oriented at an azimuth angle of 58.5°; Hole 1 had an inclination angle of 84°, and Hole 2 had an inclination angle of 80°. The first group of holes was designed with lengths of 73 m for Hole 1 and 73 m for Hole 2; the second group was designed with lengths of 105 m for Hole 3 and 104 m for Hole 4. The layout of the observation drill holes is depicted in the cross-sectional view shown in Fig. 8.

Ground borehole television survey construction locations

To conduct a comprehensive analysis of the height of the WCFZ in the No. 9 coal seam during retreat mining, drilling operations were carried out on the ground surface of the LF mine for Boreholes LD1 and LD2. The two boreholes, in the 2000 National Geocentric Coordinate System, are located at (3,025,837 m, 35,619,021 m) and (3,025,879 m, 35,619,099 m), respectively. Their elevations are 1250 m and 1215 m, with final hole depths of 440.20 m and 436.72 m, respectively. They are situated 444 m and 409 m away from the floor of the No. 9 coal seam. The specific layout of these boreholes can be seen in Fig. 9.

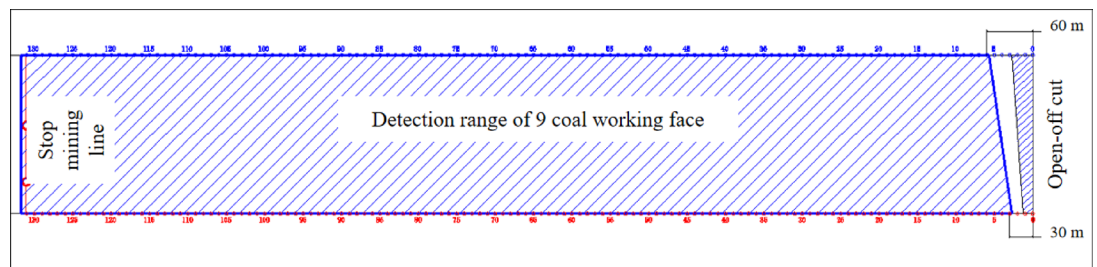


Fig. 10. Direct Current Electrical Method Exploration Layout.

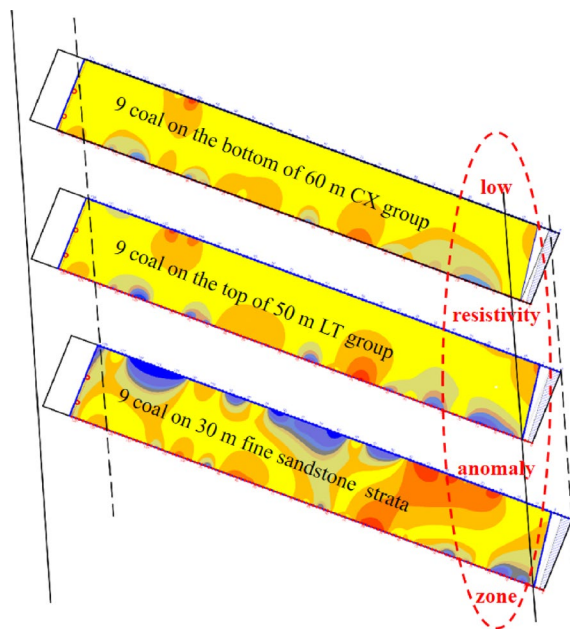


Fig. 11. Distribution of Apparent Resistivity in the Overburden.

Analysis of direct current electrical method exploration results

To comprehensively analyze the development pattern of the water-conducting fracture zone in the 1903 working face, electrical exploration points were laid out between the 1905 and 1903 working faces, with a designed spacing of 10 m between points. The starting point of the 1903 track, located 60 m back from the turning point of the 1903 track and the cut-eye, is marked as Point No. 6, and is marked along the retreat mining direction up to Point No. 131 at the end. The starting point of the 1905 track, located 30 m back from the turning point of the 1905 track and the cut-eye, is marked as Point No. 3, and is also marked along the retreat mining direction up to Point No. 131 at the end. The specific layout is shown in Fig. 10.

Based on the planar distribution of anomalies in each stratigraphic section and their vertical spatial connections, the anomalies are classified as “low-resistivity anomaly zones”. The “low-resistivity anomaly zones” refer to anomalies that occur at the same planar position across multiple stratigraphic sections, while “low-resistivity anomalies” are those that appear in only a single or a few sections. For specific classification and analysis, see Fig. 11 below.

Figure 11 illustrates the lateral variation law of the apparent resistivity values of the rock strata within the 0–60 m depth range of the roof in the No. 9 coal working face. Within the 0–60 m depth interval of the roof, a total of three anomaly zones were identified, which are inferred to be caused by the development of fracture water in the upper LT group and CX Formation strata above the No. 9 coal seam. The No. 1 low-resistivity anomaly zone is present to varying degrees at all levels within the scope of this detection, and as the detection depth increases, the range and intensity of the anomaly zone are distributed in an increasing (strengthening) - decreasing (weakening) - increasing (strengthening) pattern. This is inferred to be due to the influence of the water-rich strata in the upper LT group above the No. 9 coal seam.

On-Site observation and imaging analysis

3.5.1 Analysis of Underground Exploration Results.

Utilizing the borehole television viewing method for exploration, the LF mine’s 1903 rail bottom environment is damp, and the borehole is affected by water flow, with the hole filled with mud and water, making the

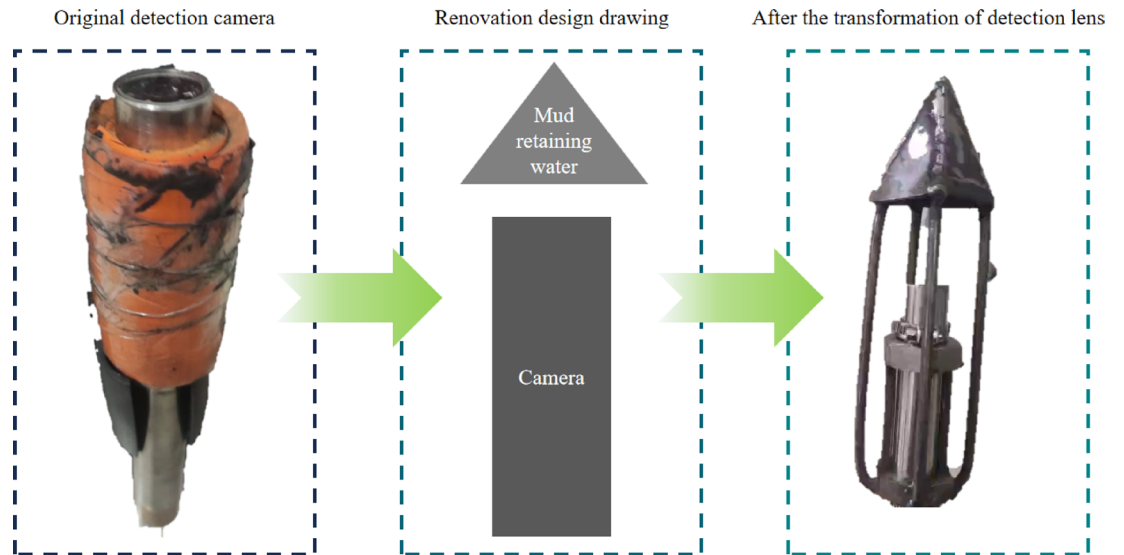


Fig. 12. Redesigned Rock Layer Detection Borehole Camera for Improved Performance.

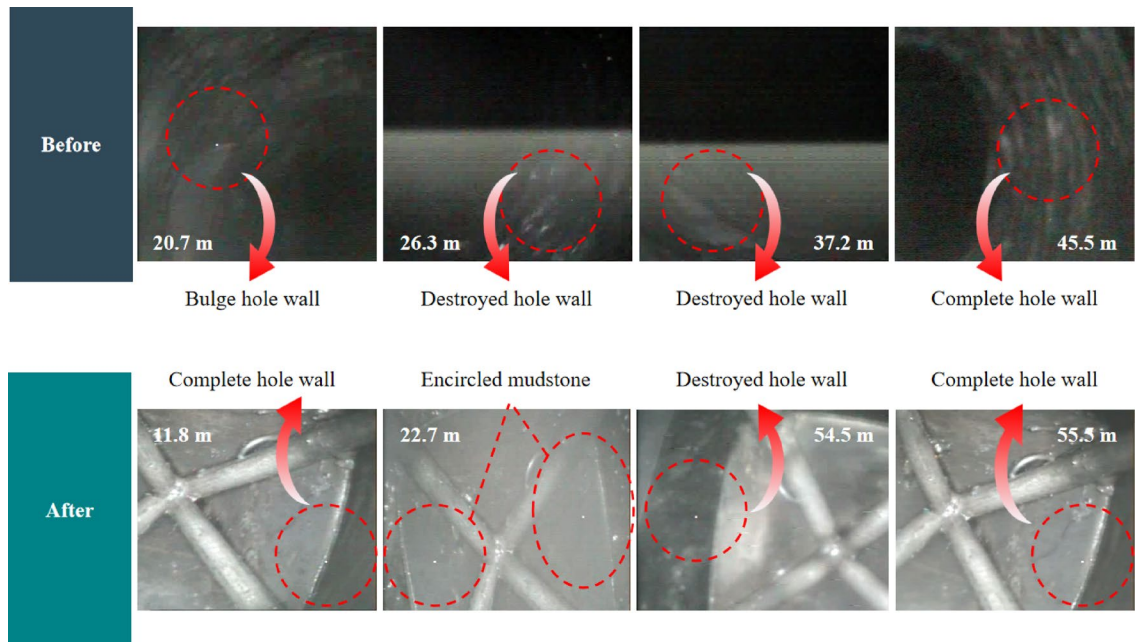


Fig. 13. Comparative Effects of the Rock Layer Detection Borehole Camera Upgrade.

observation conditions complex and the presentation quality average at best. To address this, the YTJ20 rock layer detection camera was modified, with the modifications shown in Fig. 12.

Based on Fig. 12, it can be observed that the original detection lens, due to the lack of protective measures in front, was contaminated by mud and water upon entering the borehole, leading to poor detection results. To address this issue, we have installed a mud-water shield cap in front of the detection lens and mounted four support rods on the sides of the detector. This allows for the adjustment of the distance between the mud-water shield cap and the lens, and also reduces damage to the detection camera from coal and rock during the detection process, providing a certain degree of support. The specific detection effects before and after the modification are shown in Fig. 13.

Analysis of Fig. 13 indicates that prior to the modification of the detection camera, the video effect was dim and greatly influenced by the drilling environment; after the modification, although the detection visual range was reduced, the presentation effect was improved, with brighter images and the ability to block the impact of mud and water. According to the detection results and Figure (13), at a hole depth of 11.8 m, the hole wall was intact without any signs of broken stones or fracture development; at a depth of 20.7 m, protruding rock blocks

appeared on the hole wall; from a depth of 26.3 to 37.2 m, the hole wall was damaged with broken stones; at a depth of 54.5 m, the hole wall was damaged with fractures developing; when the depth reached 55.5 m, the hole wall became intact again. In summary, around 54.5 m in depth is identified as the fracture development zone, approximately 34 m above the No. 9 coal seam floor.

Analysis of surface exploration results

From the ground construction observation holes, LD1 and LD2, mechanical core drilling and geophysical logging were employed as the primary exploration methods. During the drilling process, phenomena such as changes in the consumption of drilling fluid, variations in hole water level, and lithological identification were monitored to make a comprehensive assessment of the height of water-conducting fractures in the overburden rock of the 1903 working face of the No. 9 coal seam. The core samples are depicted in Fig. 14, and the fractures on the borehole wall are shown in Fig. 15.

Based on the on-site core sample identification, for Borehole LD1, the core samples at the intervals of 341.60–343.47 m and 368.18–369.48 m are broken. At the bottom, there is extensive development of calcite veins and a few longitudinal fractures can be observed. From 400.60 to 401.90 m, the core samples are broken and blocky. Between 408 and 417.60 m, the core samples are fractured with local development of fine fractures. The interval of 417.60–440.20 m is characterized as a broken zone. For Borehole LD2, the core samples at the interval of 345.68–346.08 m are broken. Fractures are developed, and the core samples are broken between 384.88 and 392.98 m. From 401 to 424.07 m, most of the core samples are broken, with a void observed at the interval of 415.12–415.60 m. Between 426.07 and 428.07 m, there is pulverized aluminous mudstone. Local fractures are developed, and the core samples are severely broken between 426.12 and 436.72 m.

Based on the results from the borehole televising observations, the hole walls were found to be intact at the intervals of 400.70–401.60 m and 403.00–403.70 m. Fractures were observed to develop at the intervals of 408.40–409.20 m and 415.10–415.90 m, with the hole walls regaining completeness at the interval of 435.10–436.00 m. The televising data revealed that fractures in the ground borehole are more frequently located in the lower part of the borehole, specifically within the depth range of 408.40–435.10 m.

In summary, based on the core photos from the interval of 398.18 to 402.80 m, the rock at 400.00 m is identified as grayish-black mudstone that is severely fragmented; at this depth, it is 44 m above the No. 9 coal seam floor. It can be observed that, from Borehole LD1, the top of the fracture zone is higher than 44 m from the No. 9 coal seam floor. Examining the core photographs from depths of 343.30 to 347.58 m reveals that the rock at 350 m and shallower is characterized by dark gray, thickly bedded limestone. At this depth, it is situated 59 m above the floor of the No. 9 coal seam. Observations from Borehole LD2 indicate that the top of the fracture zone is positioned at a depth less than 59 m from the No. 9 coal seam floor. Consequently, the fracture zone's development height range, as observed from the ground borehole in relation to the mining of the No. 9 coal seam, is determined to be between 44 and 59 m.

Comprehensive analysis of WCFZ development

This study investigates the damage and movement patterns of overlying strata caused by mining. The analysis primarily relies on lithological data of the overlying rock strata and field investigations of the 1903 working face. Based on these data, the distribution of key rock strata is identified and classified. Research indicates that key

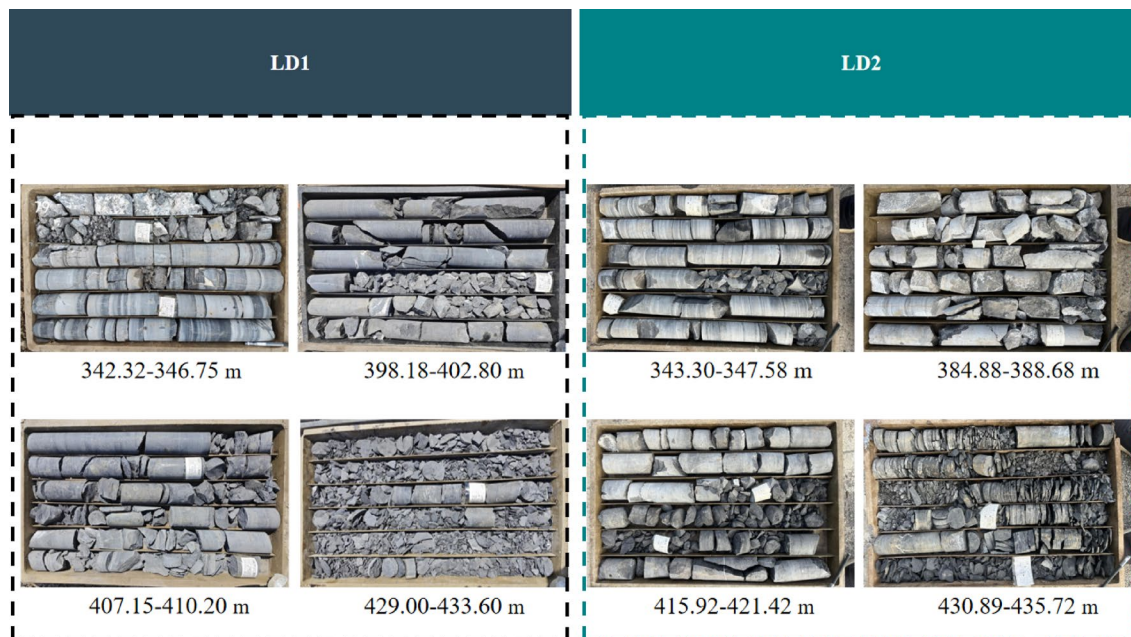


Fig. 14. Core Samples from Ground Drilling Construction Process.

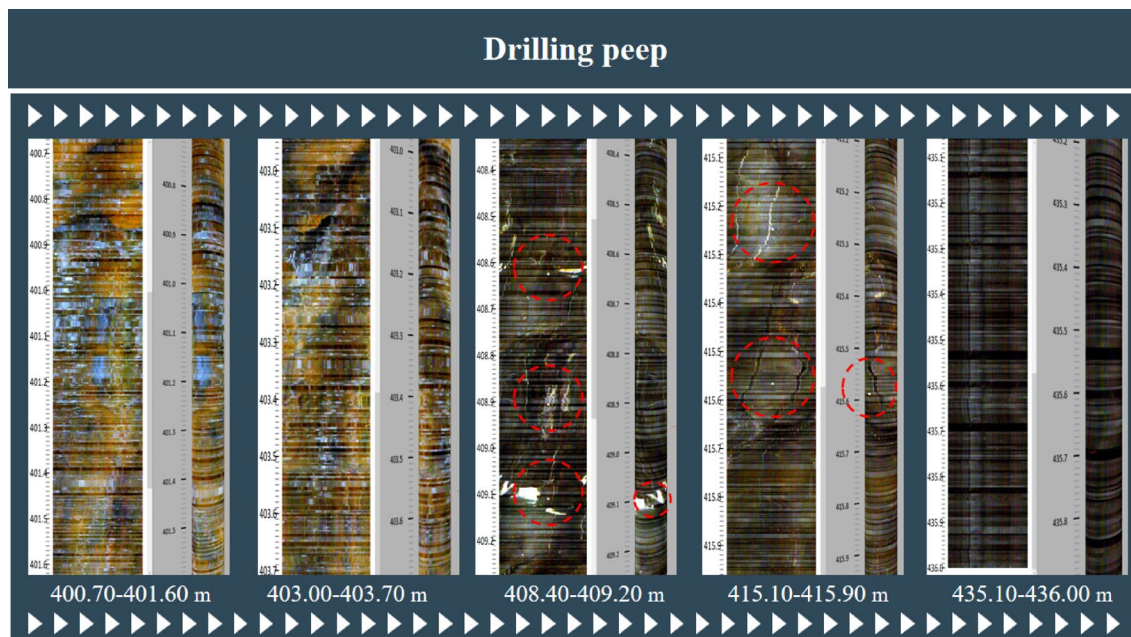


Fig. 15. Borehole Wall Fractures During Ground Drilling Construction.

rock strata distribution can be categorized into three distinct zones: the caving zone, fracture zone, and flexural subsidence zone. In the No. 9 coal seam's direct roof, which is relatively soft, underlies the LT group limestone. This limestone layer, averaging about 50 m below the coal seam top, is a major key rock stratum located within the fracture zone. Figure 1 shows the No. 9 coal seam floor is 47.37 m away from the LT group limestone. With an average thickness of 14.59 m for the LT group limestone and 24.45 m for the adjacent Upper Permian CX Formation limestone, their combined thickness of 39.04 m forms a composite limestone layer. This layer is crucial for roof movement during No. 9 coal seam mining. Below the LT group limestone lies a 4-meter-thick soft rock layer composed mainly of grayish-black silty mudstone. Prone to fracturing with the overlying limestone (the key stratum), this mudstone forms a space for water and gas accumulation. After No. 9 coal seam mining, the top of roof movement and damage is the LT group limestone, marking the upper boundary of the fracture zone. Upon thorough examination, it has been ascertained that the fracture zone's developed elevation spans from 44 to 59 m, averaging at 51.5 m, as measured perpendicularly from the base of the No. 9 coal seam. With an average extraction depth of 2.86 m, the ratio of fracture development to mining depth fluctuates between 15.39 and 20.63, averaging out at 18. The limestone layer at the base of the LT group delineates the upper limit for the fracture zone's development. From the above results, we deduced the "WCFZ" development pattern, assuming the key stratum is in the fracture zone. During No. 9 coal seam mining, roof movement and failure indicate key strata locations significantly impact the failure scope and degree. The LT group limestone, as the key stratum and fracture zone's upper boundary, determines the area's geological stability during mining. The interaction between the underlying soft rock and key stratum, forming water and gas accumulation spaces, may pose mining safety risks. Future mining plans and safety measures must fully account for these geological factors.

Improved design of borehole detector instruments

Despite the current research methods providing a comprehensive analysis of the development of WCFZ in coal seam overburdens, the performance of borehole detector instruments in complex mine shaft geological conditions and environments is not ideal^{747–49}. For instance, in some coal mines, the conductive performance of the cable may be severely hindered due to the damp and cold environment. To address this issue, it is recommended to replace the cable with one that has waterproof and cold-resistant properties. Additionally, the borehole camera is susceptible to contamination from mud and water within the borehole, affecting the image quality. To enhance the image quality, besides designing a mud-water shield cap, cameras could be installed on both sides of the detector to provide multi-angle rock layer viewing images. Such improvements could provide more comprehensive information on the lithology of the rock layers. The specific design is shown in Fig. 16:

Conclusions

(1) The overlying strata induced by mining in the 1903 working face were modeled by using the UDEC discrete element method, and the disconnection of the overlying strata and the evolution of the water-conductive fault zone were quantitatively characterized through fractal dimension analysis. Studies show that with the advancement of the working face, the fault zone of the overlying rock layer presents the development characteristics of lateral expansion and central compaction. Moreover, the fractal dimension of the water-conductive fault zone changes with the increase of the advancement distance, indicating that the development of the fault zone is closely related to the water gushing phenomenon. When the working face advances to 135 m, the limestone of Group LT

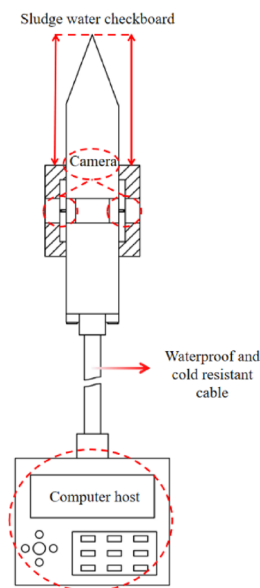


Fig. 16. Redesigned Rock Layer Detection Camera.

undergoes the maximum subsidence displacement, forming a critical disconnection space. This is a crucial period for water hazard prevention and control.

(2) Combining the data of two on-site measurement techniques, namely direct current method exploration and borehole television, and considering the hydrogeological characteristics of the 1903 working face and the development of the water-conducting fault zone induced by mining, a comprehensive analysis determined that the development height range of the water-conducting fault zone in the working face was 44 to 59 m, and the fracture ratio was 15.39 to 20.63. Silty mudstone is highly prone to rupture along with the underlying limestone layer (the critical rock layer), creating an accumulation space for water and gas.

(3) When conducting on-site exploration of the rock lithology of the roof strata in the 1903 working face, due to the complex underground environment, the initial detection results were not ideal. To enhance the detection effect, technical improvements have been made to the detection equipment, including adding a mud and water protective cover to strengthen camera protection and improve detection clarity and efficiency. In addition, further improvement measures have been proposed, such as equipping the detector with a lateral camera and using cables with waterproof, mud-proof and cold-proof properties to adapt to more complex underground environments and obtain more accurate rock layer information.

It should be noted that the research results of this article have certain limitations and applicable scopes. Due to the constraints of the selected research area and geological conditions, the conclusions and suggestions put forward are more applicable to the mining areas with similar hydrogeological characteristics and fault development patterns to the study area. For mining areas with extremely complex geological structures, such as those with multiple sets of overlapping fault zones or strong karst development, the direct application of the research results may have certain deviations. In addition, the research mainly focuses on the static characteristics and short-term dynamic changes of water conduction fault zones, and the long-term and comprehensive response law of fault zones under the influence of long-term mining activities still needs to be further verified..

In view of the above limitations, future research can be carried out in the following directions: First, conduct long-term monitoring of the dynamic evolution of water conduction fault zones, track their development characteristics in different mining stages in real time, and provide data support for dynamic water hazard early warning, so as to make up for the deficiency of insufficient research on long-term dynamic changes. Second, explore more advanced detection technologies, such as the fusion of 3D seismic exploration and intelligent sensors, to enhance the detection accuracy under complex geological conditions (especially in mining areas with extremely complex geological structures) and further optimize the performance of detection equipment, so as to expand the applicable scope of research results. Third, conduct in-depth research on the interaction mechanism between mining-induced water conduction fault zones and the groundwater hydrological system, construct a more accurate hydrogeological model, and predict the possibility of water disasters, which can provide a more reliable theoretical basis for mining areas with different geological characteristics.

Data availability

All data generated or analysed during this study are included in this published article. If you have any questions or data requirements, please contact Xijian Li at xjli1@gzu.edu.cn.

Received: 25 December 2024; Accepted: 23 July 2025

Published online: 18 November 2025

References

- Feng, C. et al. Microstructure characteristics of tectonic coal and primary coal: A case study of guizhou, China. *Nat. Resour. Res.* **32**, 2901–2926 (2023).
- Lu, Q., Qin, S., Wang, W., Wang, Q. & Kang, S. Geochemistry of late permian coals from the Yueliangtian coal deposit, guizhou: evidence of sediment source and evaluation on critical elements. *Sci. Total Environ.* **856**, 159123 (2023).
- Wu, Q. et al. Risk assessment of water inrush from aquifers underlying the Gushuyuan coal mine, China. *Mine Water Environ.* **36**, 96–103 (2017).
- Li, X. et al. Effects of mining activities on evolution of water quality of karst waters in Midwestern guizhou, china: evidences from hydrochemistry and isotopic composition. *Environ. Sci. Pollut. Res.* **25**, 1220–1230 (2018).
- Xie, H. et al. Competitive Adsorption-Penetration characteristics of Multi-Component gases in Micro-Nano pore of coal. *Chem. Eng. J.* **506**, 159965 (2025).
- Fan, H. et al. Height of Water-Conducting fractured zone in a coal seam overlain by thin bedrock and Thick clay layer: A case study from the Sanyuan coal mine in North China. *Environ. Earth Sci.* **79**, 125 (2020).
- Hu, X. & Zhang, Q. Mine water treatment, resource utilization and prospects in coal mining areas of Western China. *Mine Water Environ.* **43**, 210–230 (2024).
- Wang, F., Tu, S., Zhang, C., Zhang, Y. & Bai, Q. Evolution mechanism of Water-Flowing zones and control technology for Longwall mining in shallow coal seams beneath gully topography. *Environ. Earth Sci.* **75**, 1309 (2016).
- Lu, C., Xu, J., Li, Q., Zhao, H. & He, Y. Research on the development law of Water-Conducting fracture zone in the combined mining of jurassic and carboniferous coal seams. *Applied Sciences.* **12**(21), 11178 (2022).
- Li, Y. et al. Study on the failure characteristics of overburden and the evolution law of seepage field in deep buried Thick coal seam under aquifers. *Nat. Hazards.* **118**, 1035–1064 (2023).
- Ning, J., Wang, J., Tan, Y. & Xu, Q. Mechanical mechanism of overlying strata breaking and development of fractured zone during Close-Distance coal seam group mining. *Int. J. Min. Sci. Technol.* **30**, 207–215 (2020).
- Lu, C., Zhang, X. & Han, L. Study on movement law of overburden strata and fracture zone height in deep mining work face. *Front Earth Sci.* **11**, (2023).
- Li, J., He, Z., Piao, C., Chi, W. & Lu, Y. Research on subsidence prediction method of Water-Conducting fracture zone of overlying strata in coal mine based on grey theory model. *Water.* **15**(23), 4177 (2023).
- Zhou, Y. & Yu, X. Study of the evolution of Water-Conducting fracture zones in overlying rock of a fully mechanized caving face in gently inclined Extra-Thick coal seams. *Applied Sciences.* **12**(18), 9057 (2022).
- Chang, X., Wang, M., Zhu, W., Fan, J. & Liu, M. Study on height development characteristics of water-Conducting fracture zone in fully mechanized mining of shallow Thick coal seam under water. *Sustainability.* **15**(9), 7370 (2023).
- Wan, F., Zhang, H., Zhou, P. & Guo, J. Determination of Water-Proof Coal (Rock) Pillar Height in Mining Coal Seam Group Under Water-Bearing Rock Stratum. *Shock Vib.* 6699726 (2021). (2021).
- Long, T., Hou, E., Xie, X., Fan, Z. & Tan, E. Study on the damage characteristics of overburden of mining roof in deeply buried coal seam. *Sci. Rep.* **12**, 11141 (2022).
- Sun, D., Li, X., Zhu, Z., Li, Y. & Cui, F. Height of the Fractured Zone in Coal Mining Under Extra-Thick Coal Seam Geological Conditions. *Adv. Civ. Eng.* 9998545 (2021). (2021).
- Li, B., Wu, H. & Li, T. Height prediction of Water-Conducting fractured zone under fully mechanized mining based on weighted multivariate nonlinear regression. *J. Min. Saf. Eng.* **39**, 536–545 (2022).
- Cao, J., Su, H., Wang, C. & Li, J. Research on the evolution and height prediction of Wcfz in shallow close coal seams mining. *Geomech. Geophys. Geo-Energy Geo-Resour.* **9**, 128 (2023).
- Li, Y., Xiao, J., Wang, Y. & Deng, C. Numerical simulation investigation on fracture propagation of fracturing for crossing coal seam roof. *Processes.* **10**(7), 1296 (2022).
- Qi, Y., Wang, W., Ge, J., Yang, Z. & Qi, Q. Development characteristics of the rock fracture field in strata overlying a mined coal seam group. *Plos One.* **17**, e0268955 (2022).
- Chen, Y. & Zhu, S. Determination of caved and Water-Conducting fractured zones of two soft and one hard unstable coal seam. *Acta Geod. Geophys.* **55**, 451–475 (2020).
- Yang, S., Xu, N., Liu, H., Zhang, X. & Mei, S. Research and application of ‘three zones’ range within overlying strata in Goaf of steep coal seam. *Front Energy Res.* **12**, (2024).
- Dong, Y. et al. Fine detection on water abundance of sandstone by joint inversion of seismic and csamt: A case study in the Western Ordos basin, China. *Acta Geophys.* **70**, 2045–2056 (2022).
- , Z. et al. Surface-to-Underground transient electromagnetic detection of Water-Bearing goaves. *Ieee Trans. Geosci. Remote Sens.* **57**, 5303–5318 (2019).
- Ding, K. et al. Study On the Development Height of Overburden Water-Flowing Fracture Zone of the Working Face. *Geofluids.* 5570884 (2021). (2021).
- Shang, Y., Zhang, L., Kong, D., Wang, Y. & Cheng, Z. Overlying strata failure mechanism and gas migration law in close distance outburst coal seams: A case study. *Eng. Fail. Anal.* **148**, 107214 (2023).
- ZHOU, Z. et al. Quantifying Rough Fracture Behaviors in Gas-Bearing Coal Seam: A Fully Coupled Fractal Analysis. *Fractals.* 2450085 (2024).
- Hou, E., Wen, Q., Ye, Z., Chen, W. & Wei, J. Height prediction of Water-Flowing fracture zone with a Genetic-Algorithm Support-Vector-Machine method. *Int. J. Coal Sci. Technol.* **7**, 740–751 (2020).
- Xu, C., Zhou, K., Xiong, X., Gao, F. & Zhou, J. Research on height prediction of Water-Conducting fracture zone in coal mining based on intelligent algorithm combined with extreme boosting machine. *Expert Syst. Appl.* **249**, 123669 (2024).
- Y., Z., C., F., H., K. & S., Z. The Height of Water-Conducting Fractured Zone Prediction Using Principal Component Analysis and Relevance Vector Machine. *International Conference on Algorithms, Data Mining, and Information Technology (ADMIT)*, 2022:196–201., 2022:196–201. (2022).
- He, X., Zhao, Y., Zhang, C. & Han, P. A model to estimate the height of the Water-Conducting fracture zone for Longwall panels in Western China. *Mine Water Environ.* **39**, 823–838 (2020).
- Liu, Y., Liu, Q., Li, W., Li, T. & He, J. Height of Water-Conducting fractured zone in coal mining in the Soil-Rock composite structure overburdens. *Environ. Earth Sci.* **78**, 242 (2019).
- Sun, J. & Miao, X. Water-Isolating capacity of an inclined coal seam floor based on the theory of Water-Resistant key strata. *Mine Water Environ.* **36**, 310–322 (2017).
- Yan, H., Zhang, J., Li, L., Feng, R. & Li, T. Prediction of upper limit position of bedding separation overlying a coal roadway within an Extra-Thick coal seam. *J. Cent. South. Univ.* **25**, 448–460 (2018).
- He, J. et al. A method for predicting the Water-Flowing fractured zone height based on an improved key stratum theory. *Int. J. Min. Sci. Technol.* **33**, 61–71 (2023).
- Xingping, L. et al. Evolution characteristics of water flowing 674 fracture in shallow buried coal seam in water abundance gully Valley area. *Coal Sci. Technol.* **52**, 1–11 (2024).
- Xingping, L. et al. Study on development law of Water-Conducting fractures in overlying strata of three soft coal seam mining under Thick loose layers. *J. Rock. Mech. Eng.* **40**, 1739–1750 (2021).
- Zhang, Y., Tu, S., Bai, Q. & Li, J. Overburden fracture evolution laws and Water-Controlling technologies in mining very Thick coal seam under Water-Rich roof. *Int. J. Min. Sci. Technol.* **23**, 693–700 (2013).

41. , S. B. et al. Monitoring direct current resistivity during coal mining process for underground water detection: an experimental case study. *Ieee Trans. Geosci. Remote Sens.* **60**, 1–8 (2022).
42. Wang, Y. et al. A case study of direct current resistivity method for disaster water source detection in coal mining. *Elektron Elektrotech.* **27**, 41–48 (2021).
43. Zhao, E., Li, K., Yang, X. & Deng, N. Speculum Observation and Trajectory Measurement in Gas Extraction Drilling: A Case Study of Changling Coal Mine. *Geofluids.* 5545067 (2021). (2021).
44. Liu, C. et al. Intelligent recognition and identification of fracture types and parameters for borehole images based on developed convolutional neural networks and Post-Processing. *Eng. Fract. Mech.* **292**, 109624 (2023).
45. Wood, D. A. Expanding role of borehole image logs in reservoir fracture and heterogeneity characterization: A review. *Advances Geo-Energy Research.* **12**(3), 194–204 (2024).
46. Cai, J., Li, X., Guo, L., Xue, H. & Xu, B. Fracture Development and Multifield Coupling Evolution Law of Soft Overburden Rock in a Medium-Thick Coal Seam Mine. *Geofluids.* 6371887 (2022). (2022).
47. Hu, W. & Zhao, C. Evolution of water hazard control technology in china's coal mines. *Mine Water Environ.* **40**, 334–344 (2021).
48. Wang, C., Wang, Y., Zou, X., Han, Z. & Zhong, S. Study of a borehole panoramic stereopair imaging system. *Int. J. Rock. Mech. Min. Sci.* **104**, 174–181 (2018).
49. Zhao, J. et al. Rock fracturing observation based on microseismic monitoring and borehole imaging: in situ investigation in a large underground cavern under high geostress. *Tunn. Undergr. Space Technol.* **126**, 104549 (2022).

Acknowledgements

This work was supported by the National Nature Science Foundation of China (Grant No. 52164015, 52364009), the Science and Technology Funding Projects of Guizhou Province, Grant/Award No. [2022]231, Guizhou Provincial Basic Research Program (Natural Science) (No. Qian Ke He Ji Chu - ZK [2024] Yi Ban 098)

This study is partially based on materials sourced from the “LF Coal Mine Two-Belt Hole Construction Summary Report” and the “1905 Working Face Direct Current Electric Method Exploration Results Report.” These two reports were respectively compiled by the Geological and Mineral Construction Branch of Shandong Energy Construction Engineering Group Co., Ltd. and Xi’an Kun’an Surveying and Mapping Technology Co., Ltd., and were provided by Guizhou Jinsha Longfeng Coal Industry Co., Ltd. During the research process, we extend our sincere gratitude to the multiple cooperating units for their substantial support.

Author contributions

E X, C X: Methodology, Software, Writing - Original draft, X L,: method, financial support, W Z, X Y, Y P, Z D and C Z assisted in the site operation and data, SK C assisted in the experiment, method, financial support. All authors reviewed the manuscript.

Declarations

Competing interests

The authors declare no competing interests.

Additional information

Correspondence and requests for materials should be addressed to X.L.

Reprints and permissions information is available at www.nature.com/reprints.

Publisher’s note Springer Nature remains neutral with regard to jurisdictional claims in published maps and institutional affiliations.

Open Access This article is licensed under a Creative Commons Attribution-NonCommercial-NoDerivatives 4.0 International License, which permits any non-commercial use, sharing, distribution and reproduction in any medium or format, as long as you give appropriate credit to the original author(s) and the source, provide a link to the Creative Commons licence, and indicate if you modified the licensed material. You do not have permission under this licence to share adapted material derived from this article or parts of it. The images or other third party material in this article are included in the article’s Creative Commons licence, unless indicated otherwise in a credit line to the material. If material is not included in the article’s Creative Commons licence and your intended use is not permitted by statutory regulation or exceeds the permitted use, you will need to obtain permission directly from the copyright holder. To view a copy of this licence, visit <http://creativecommons.org/licenses/by-nc-nd/4.0/>.

© The Author(s) 2025